Environmental Science & Technology

Article

Cite This: Environ. Sci. Technol. 2019, 53, 6972−6980

pubs.acs.org/est

Activation of Peroxymonosulfate by Oxygen Vacancies-Enriched Cobalt-Doped Black TiO_2 Nanotubes for the Removal of Organic Pollutants

Jonghun Lim, Yang Yang, and Michael R. Hoffmann*

Linde + Robinson Laboratories, California Institute of Technology, Pasadena, California 91125, United States

Supporting Information

ABSTRACT: Cobalt-mediated activation of peroxymonosulfate (PMS) has been widely investigated for the oxidation of organic pollutants. Herein, we employ cobalt-doped Black TiO_2 nanotubes (Co-Black TNT) for the efficient, stable, and reusable activator of PMS for the degradation of organic pollutants. Co-Black TNTs induce the activation of PMS by itself and stabilized oxygen vacancies that enhance the bonding with PMS and provide catalytic active sites for PMS activation. A relatively high electronic conductivity associated with the coexistence of Ti^{4+} and Ti^{3+} in Co-Black TNT enables an efficient electron transfer between PMS and the catalyst. As a result, Co-Black TNT is an effective catalyst for PMS activation, leading to the degradation of selected organic pollutants when compared to other TNTs (TNT, Co-TNT, and Black TNT) and other Co-based materials (Co_3O_4, Co-TiO_2, $CoFe_2O_4$, and Co_3O_4/rGO). The observed organic compound degradation kinetics are retarded in the presence of methanol and natural organic matter as sulfate radical scavengers. These results demonstrate that sulfate radical is the primary oxidant generated via PMS activation on Co-Black TNT. The strong interaction between Co and TiO_2 through Co−O−Ti bonds and rapid redox cycle of Co^{2+}/Co^{3+} in Co-Black TNT prevents cobalt leaching and enhances catalyst stability over a wide pH range and repetitive uses of the catalyst. Electrode-supported Co-Black TNT facilitates the recovery of the catalyst from the treated water.

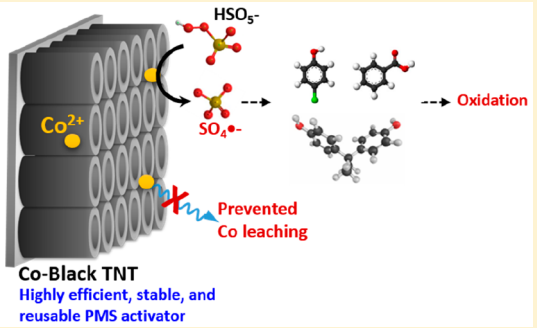

INTRODUCTION

Peroxymonosulfate (PMS)-activated oxidation has been investigated for water treatment and soil remediation through nonradical and radical pathways.[1−5] A nonradical mechanism involves the direct electron transfer from organic electron donor to PMS on catalyst surfaces (e.g., carbon nanotubes (CNT) and reduced graphene oxide, rGO) leading to the oxidation of organic compounds with the formation of sulfate ($E^0(HSO_5^-/SO_4^{2-})$ = 1.75 V_{NHE}).[6−8] On the other hand, free radical pathways involve the formation of sulfate radical anions ($E^0(HSO_5^-/SO_4^{\bullet-})$ = 2.43 V_{NHE}) generated from PMS by catalysts coupled with an external energy input to cleave the peroxide bond.[9] The free-radical mechanism has attracted more attention, compared to the nonradical mechanism, because it can treat a broad spectrum of recalcitrant organic pollutants, given the high oxidizing potential of $SO_4^{\bullet-}$ over a broad range of pH.[10] A variety of methods have been employed to generate $SO_4^{\bullet-}$ via PMS activation.[11−19] Transition-metal ions with multiple valence state are most frequently used for activation of PMS without the need for external energy inputs (e.g., UV light and electricity).[20]

Cobalt ion (Co^{2+}) is often used as a PMS activator over a wide range of pH.[1] However, concerns have been raised about the use of Co^{2+} in water remediation, because of various human health concerns (e.g., asthma, pneumonia, and other lung problems).[21,22] As a result, heterogeneous cobalt-based catalysts have been developed to avoid the potential problems of using homogeneous solutions of soluble cobalt. For example, Co_3O_4 (20 nm)/PMS has been shown to be better than homogeneous Co^{2+}/PMS activation for organic compound degradation, in part, because there is minimal leaching of Co^{2+} from Co_3O_4 at circum-neutral pH.[23,24] Other heterogeneous Co-containing materials have been proposed for PMS activation such as $Co_xFe_{3-x}O_4$ and $Co_xMn_{3-x}O_4$ without Co^{2+} leaching, because of the strong interactions between Co and the doped transition-metal ions.[25,26] When Co-based catalysts have been embedded into the surface of supports such as activated carbon, rGO, SBA-15, and metal organic frameworks (MOFs) PMS activation efficiencies and stabilities were improved.[27−29] Even though many Co-based catalysts have been developed to activate PMS, the practical applications of heterogeneous slurry systems are often limited by the need for catalysts recovery step. Catalysts deposited on suitable substrates (e.g., glass, silicon, and metal foams) can be easily recovered and reused without the need for physical separation and recovery step such as filtration, centrifugation, or magnetic recovery.[30,31] However, these methods are often

Received: March 7, 2019
Revised: May 10, 2019
Accepted: May 15, 2019
Published: May 15, 2019

DOI: 10.1021/acs.est.9b01449
Environ. Sci. Technol. 2019, 53, 6972−6980

costly and limited for long-term usage, because of the use of adhesive materials or organic binders that limit the contact between catalysts and target substrates.

TiO_2 nanotube arrays (TNTs) have been used for photocatalytic and electrochemical applications, because of their fundamental properties, such as high surface areas and open-channel structures that facilitate mass transfer of the target substrates.[32,33] In addition, TNTs are synthesized on the surface of Ti-metal plates by anodization without the need for adhesives or organic binders.[34] Despite these advantages, the applications of TNTs are often restricted by their low electrical conductivity.[35] The electrical conductivity of TNTs can be enhanced by self-doping that induces a partial reduction of Ti^{4+} to Ti^{3+}, together with the formation of oxygen vacancies.[36] Therefore, the resultant Black TNTs have been studied for various applications.[37] Black TNTs have some desirable properties that include high surface areas, open-channel structures, high electrical conductivity, chemical stability, easy to synthesize, and readily immobilization on support matrices.

In this study, we employed cobalt-doped Black TiO_2 nanotubes (Co-Black TNT) as an efficient, stable, and reusable PMS activator for the degradation of organic pollutants. Co-Black TNT is shown to outperform other TNTs composites (bare TNT, Co-TNT, and Black TNT) and other Co-based activators (e.g., Co_3O_4, Co-TiO_2, $CoFe_2O_4$, and Co_3O_4/rGO) for PMS activation. The mechanism of PMS activation is investigated using probe reagents and electron paramagnetic resonance (EPR). We also discuss the practical merits of directly growing Co-Black TNT on Ti plates without the need of additional adhesive materials or organic binders. The attached growth feature allows for the reuse of the catalysts without separation and recovery steps.

MATERIALS AND METHODS

Chemicals and Materials. Chemical reagents used in this study were as follows: potassium peroxymonosulfate ($2KHSO_5{\cdot}KHSO_4{\cdot}K_2SO_4$, available as OXONE, PMS; Aldrich), 4-chlorophenol (4-CP, Sigma−Aldrich), bisphenol A (BPA, Aldrich), phenol (J.T. Baker), benzoic acid (BA, EMD Millipore), methanol (J.T. Baker), *tert*-butanol (*t*-BuOH, Aldrich), phosphate buffer solution (pH 7.2, Sigma−Aldrich), 5-*tert*-butoxycarbonyl 5-methyl-1-pyrroline-*N*-oxide (BMPO, ENZO Life Sciences, Inc.). All chemical reagents were used as received without any purification. Deionized water (DW) was used as a solution and prepared using a Millipore system (≥18 MΩ, Milli-Q). Self-organized amorphous TNT electrodes were fabricated and simultaneously immobilized on a Ti plate by an electrochemical anodization method. The growth TNTs on a Ti-metal plate proceeds as follows: (i) formation of non-conductive thin Ti oxide layer on a Ti plate, (ii) an anodic oxidation of Ti ($Ti \rightarrow Ti^{n+} + ne^-$) at a sufficiently higher applied voltage coupled with the dissolution of Ti^{n+} ions in the electrolyte to form localized pits (a compact Ti oxide), and (iii) achieving a balance between Ti^{n+} solvation and oxide formation in order to form the nanotube structures.[38] Ti-metal plates were anodized at +42 V in an ethylene glycol (EG) electrolyte on solution composed of 0.25 wt % NH_4F and 2 wt % H_2O for 6 h.[39] After anodization, amorphous TNT was dip-coated in a 250 mM $Co(NO_3)_2$ ethanol solution for 1 min, pulled up at the rate of 10 mm/min, and dried at room temperature for 2 min. These processes were repeated three times. Bare- and Co-loaded-amorphous TNT were annealed at 450 °C in air for 1 h to make bare- and Co-TNT, respectively. To form Black TNT and Co-Black TNT, the bare- and Co-loaded amorphous TNTs were annealed at 450 °C in a stream of 5% H_2/Ar for 30 min. A higher level Co-doping of Black TNT (containing, i.e., Co-Black TNT/CoO_x) was prepared by drop-casting 125, 250, and 500 mM of the $Co(NO_3)_2$/ethanol solution. The Co loading was determined to be 0.54 μmol/cm^2 for Co-Black TNT and 3.12, 4.20, and 7.11 μmol/cm^2 for Co-Black TNT/CoO_x, using inductively coupled plasma mass spectrometry (ICP-MS). Four samples (Co_3O_4, Co_3O_4/rGO, Co-TiO_2, and $CoFe_2O_4$) were prepared for comparison with Co-Black TNT (see experimental details in the Supporting Information for information regarding the preparation of four control samples).

Characterization. The crystalline phase was identified via X-ray diffraction (XRD) (PANalytical X'Pert Pro). The surface chemical composition was analyzed using X-ray photoelectron spectroscopy (XPS, Surface Science M-Probe ESCA/XPS). Scanning electron microscopy (SEM) (Zeiss, Model 1550VP) coupled with energy-dispersive X-ray spectroscopy (EDX) were used to obtain SEM and EDX images. The surface charge of Co-Black TNT was analyzed using an electrophoretic light scattering spectrophotometer (ELSZ-1000).

Experimental Procedures and Analyses. The prepared TNT electrodes were dipped into distilled water. An aliquot of the organic substrate stock solution and the PMS stock solution was added into a magnetically stirred reactor. The solution was typically buffered at pH 7.2 using phosphate buffer pair (3 vol %). The 4-CP removal activity was not changed in unbuffered solution, which demonstrates the marginal effect of phosphate buffer (Figure S1 in the Supporting Information) in the Co-Black TNT/PMS reaction system. To evaluate pH effects, the experimental solution was unbuffered, and the initial pH values (3, 5, 9, and 11) were established using a standard solution of either $HClO_4$ or NaOH. Sample aliquots versus time were withdrawn from the reactor using a 1 mL pipet and injected into a 2 mL amber glass vial containing excess methanol (0.1 M) to inhibit the reaction of any residual radicals.

The concentrations of the organic substrates were determined using a high-performance liquid chromatography (HPLC) system (Agilent 1100 series) that was equipped with a Zorbax XDB column. The eluent consisted of a binary mobile phase of acetonitrile and formic acid (10%:90% for phenol, 4-CP, and BA and 30%:70% for BPA). Chloride ion concentrations produced via dechlorination of 4-CP were monitored using an ion chromatograph (IC, Dionex, USA) with an anion-exchange column (Ionpac AS 19). The removal of total organic carbon (TOC) was determined using a TOC analyzer (Aurora TOC). PMS concentrations were spectrophotometrically determined by following a standard method.[40] For electron paramagnetic resonance (EPR) analyses, 5-*tert*-butoxycarbonyl 5-methyl-1-pyrroline-*N*-oxide (BMPO) was used as a spin-trapping agent for $SO_4^{\bullet -}$. The EPR spectra were recorded on a Bruker EMX X-band CW-EPR spectrometer using the following conditions: microwave power = 20 mW, microwave frequency = 9.836, and at room temperature. The concentration of Co leached in the solution was determined by ICP-MS.

Electrochemical Measurements. Electrochemical impedance spectroscopy (EIS) and Mott−Schottky plots were measured using a Biologic VSP-300 potentiostat. TNT electrodes, stainless steel, and Ag/AgCl were utilized as the

DOI: 10.1021/acs.est.9b01449
Environ. Sci. Technol. 2019, 53, 6972−6980

working electrode, a counter electrode, and a reference electrode, respectively. The electrodes were immersed in 0.1 M $NaClO_4$ solution. The EIS plots were obtained over the frequency range of 200 kHz to 0.1 Hz. Mott−Schottky analysis was performed using a potential range from −1.0 V to 1.0 V (vs Ag/AgCl) at a frequency of 200 kHz and alternating current (AC) voltage of 25 mV.

RESULTS AND DISCUSSION

Physicochemical Properties of Synthesized TNTs. The product TNT samples were characterized by using XRD and SEM and the distribution of elements within Co-Black TNT was analyzed by EDX (see Figures S2−S4 in the Supporting Information and accompanying discussion in the Supporting Information for details).

The oxidation states and oxygen vacancies were analyzed by XPS spectra (Figure 1). The two peaks corresponding to Co $2p_{3/2}$ and $2p_{1/2}$, centered at 781 and 797 eV, respectively, were confirmed in the Co 2p XPS spectra of Co-doped TNTs,[41] and they were shifted to a higher binding energy, compared to the spectra of Co_3O_4 (Figure 1a). This result indicates that Co^{2+} only is present in Co-doped TNTs, whereas the mixed states of Co^{2+} and Co^{3+} are contained in Co_3O_4.[42] The both Co 2p peaks were not observed in bare- and Black-TNT (data not shown). We analyzed the XPS spectra of O 1s to confirm the oxygen vacancies in the prepared samples. The O 1s XPS spectra were deconvoluted with three major peaks, located at 529.9, 531.8, and 532.6 eV (Figure 1b), which correspond to lattice oxygen species (O_2^-), adsorbed oxygen (e.g., O_2^{2-} and O^-), and hydroxyl groups (OH^-), respectively.[43,44] The peak at 531.8 eV is closely related to the oxygen vacancies, since the molecular oxygen is dissociatively adsorbed on surficial oxygen vacancies.[41,42] The relative concentrations of the oxygen vacancies were estimated indirectly, using the peak at 531.8 eV. Co-Black TNT (25%) was found to have a higher relative concentration of oxygen vacancies, compared to Black TNT (21%), Co-TNT (17%), and bare TNT (11%). The Ti 2p XPS measurement (Figure 1c) confirmed the presence of Ti^{3+} on the surface of doped TNTs. The typical two peaks were observed at binding energies of 464.8 (for Ti $2p_{1/2}$) and 458.9 eV (for Ti $2p_{3/2}$) in bare- and Co-TNT,[45] whereas they were shifted to a lower binding energy in hydrogenated TNTs (Black and Co-Black TNT), because of a partial reduction of Ti^{4+} to Ti^{3+}.

The electrochemical impedance spectroscopy (EIS) was used to evaluate the charge-transfer resistances of synthesized TNTs. A smaller arc size in a EIS Nyquist plot correlates to a smaller resistance to charge transfer on the surface of electrode.[46] The arc size in EIS Nyquist plots decreased in the following order: bare TNT > Co-TNT > Black TNT > Co-Black TNT (see Figure 2a). This result suggests that the electron transfer in the Co-Black TNT is more efficient than that for the other TNTs. Electron transfer efficiency is confirmed by Mott−Schottky analysis, as shown in Figure 2b. The Co-Black TNT gave a flat slope, compared to the other TNTs. This behavior also indicates enhanced electron transport.[35] The presence of oxygen vacancies and Ti^{3+} as donor states below conduction band of Co-Black TNT results in a redistribution of excess electrons between the nearest neighboring Ti atoms and oxygen vacancy sites to achieve charge balance, which, in turn, increases the charge carrier density.[47] As a result, the electrical conductivity of Co-Black TNT is enhanced.

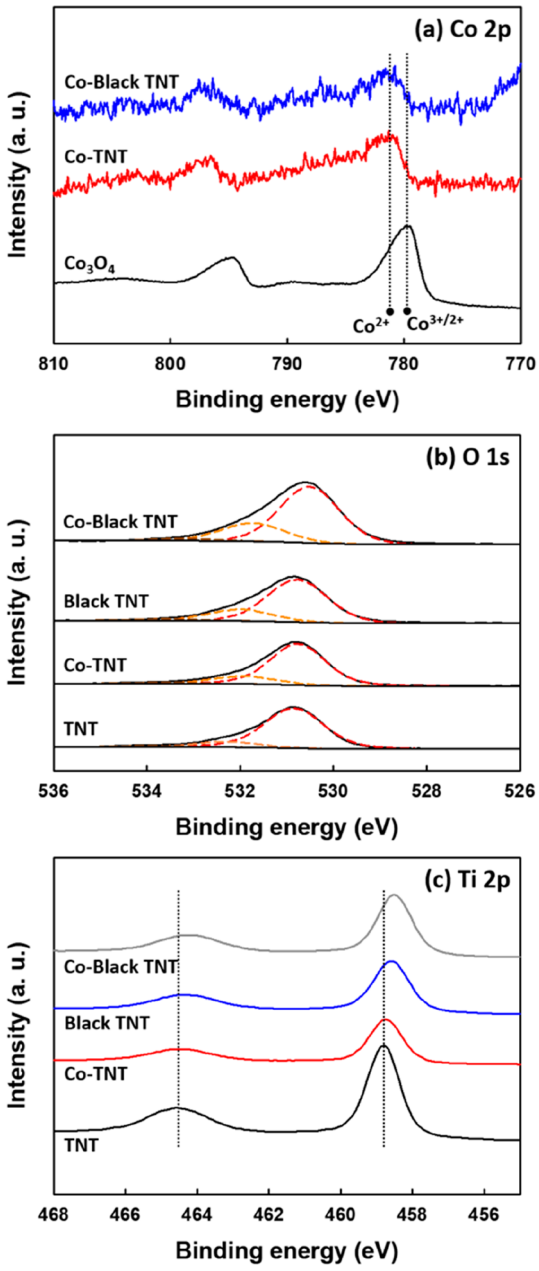

Figure 1. XPS spectra of (a) Co 2p, (b) O 1s, and (c) Ti 2p signals in Co-Black TNT, Co-TNT, Black TNT, bare TNT.

PMS Activation by TNTs. The Co-Black TNT electrodes had a higher efficiency for 4-CP degradation, stoichiometric Cl^- production, and TOC removal, compared to the other TNTs (e.g., bare-, Co-, and Black-TNT) (Figures 3a−c). However, in the absence of the catalyst (Co-Black TNT) or PMS, there was negligible 4-CP degradation (see Figure S5 in the Supporting Information). This implies that 4-CP is mainly degraded via PMS activation on the Co-Black TNT surface. 4-CP degradation by bare TNT was insignificant, because PMS cannot be activated in the absence of Co^{2+}. Despite the lack of Co^{2+} in Black TNT, 49% of the 4-CP was decomposed over the same time frame. This result may be ascribed to that Black TNT with a high conductivity (see Figure 2) mediates a facial electron transfer from 4-CP to PMS (i.e., nonradical mechanism). The activation of PMS in Co-TNT markedly accelerated 4-CP degradation and it was further enhanced in

DOI: 10.1021/acs.est.9b01449
Environ. Sci. Technol. 2019, 53, 6972−6980

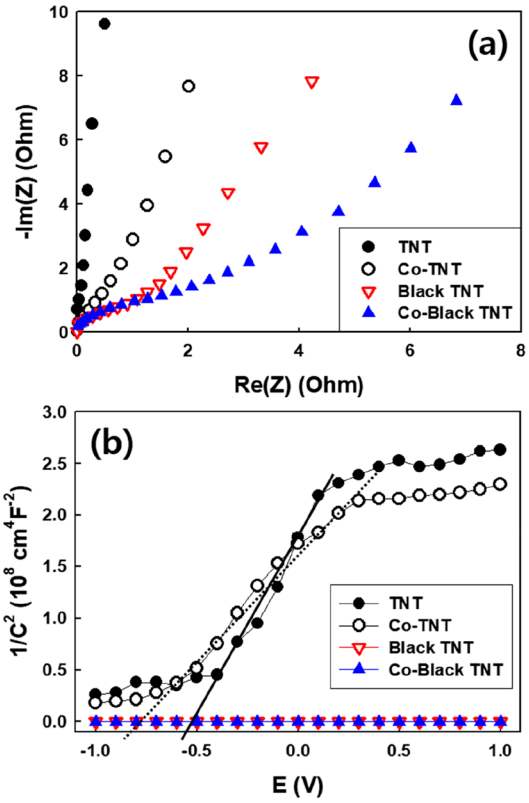

Figure 2. (a) Nyquist plots of TNT, Co-TNT, Black TNT, and Co-Black TNT. Nyquist plots were obtained in the frequency range of 200 kHz to 0.1 Hz. (b) Mott–Schottky plots in electrochemical impedance spectroscopy. The Mott–Schottky plots were measured at a fixed frequency of 200 kHz in aqueous $NaClO_4$ solution (0.1 M).

Co-Black TNT, which is ascribed to superior properties of Co-Black TNT for PMS activation.

PMS activation is initiated by the adsorption of PMS on the surface of heterogeneous catalysts (e.g., metal oxides) and the charge transfer between catalysts and PMS generates $SO_4^{\bullet -}$ that is subsequently desorbed from the catalyst surface into the aqueous solution for degrading organic pollutants.[48] In addition, a fast redox cycle (M^{n+}/M^{n+1}) of metal ions located on the catalyst surface enhances the generation of $SO_4^{\bullet -}$.[48] Therefore, the heterogeneous catalysts should have a strong interaction with PMS and the organic substrates coupled with a high electrical conductivity that results in a fast redox cycling of key metal ions to efficiently activate PMS. Co-Black TNT contains a significant number of oxygen vacancies (see Figure 1b) that allow for the facile chemical bonding of PMS.[48] Oxygen vacancies, which are also efficient oxygen ion conductors, allow for the facile redox cycling of Co^{2+}/Co^{3+} with PMS (see eqs 1 and 2).[48] In contrast, Co_3O_4 has a low oxygen ion conductivity, which limits its activity and stability.[49]

$$Co^{2+} + HSO_5^- + V_O^{\cdot\cdot} \rightarrow Co^{3+} + SO_4^{\cdot -} + H^+ + O_O^{\times} \quad (1)$$

$$Co^{3+} + HSO_5^- + H^+ + O_O^{\times} \rightarrow Co^{2+} + SO_5^{\cdot -} + H_2O + V_O^{\cdot\cdot} \quad (2)$$

where $V_O^{\cdot\cdot}$ and $O_O^{\times}$ represent a doubly charged oxygen vacancy and the oxygen ion in an oxygen site on the Co-Black TNT surface, respectively. In addition, the presence of defect sites such as oxygen vacancies and Ti^{3+} enables a faster surface reaction via a higher electron transfer capability of Co-Black TNT, as demonstrated by the electrochemical analysis (see Figure 2).[34,35] As a result, the PMS activation efficiency of Co-Black TNT was much higher than that of other TNTs (see Figures 3a–c). However, the degradation of 4-CP was reduced with increasing Co concentration in the Co-Black TNT (Figure S6 in the Supporting Information). This result is attributed to an amorphous CoO_x layer formed on the top of Co-Black TNT (Figure S7 in the Supporting Information) that blocks the open-channel structure of the nanotubes, effectively reducing the electrical conductivity (Figure S8 in the Supporting Information) and inhibiting the mass transfer of PMS and substrates.[32] The characteristic peaks of cobalt oxide were not observed in the XRD patterns of Co-Black TNT/CoO_x (data not shown), which implies that the CoO_x layer is amorphous. We further compared the 4-CP removal activity of Co-Black TNT with Co_3O_4, Co-TiO_2, $CoFe_2O_4$, and Co_3O_4/rGO, as shown in Figure 3d. The 4-CP removal rate was the highest for Co-Black TNT, with a pseudo-first-order rate constant of 0.28 min^{-1}. In comparison, the corresponding rate constants for the other cobalt materials were as follows: for Co_3O_4/rGO, k = 0.18 min^{-1}; for $CoFe_2O_4$, k = 0.17 min^{-1}; for Co_3O_4, k = 0.13 min^{-1}; and for Co-TiO_2, k = 0.11 min^{-1}.

The Co-Black TNT/PMS system also had a relatively high efficiency for the degradation of phenol and bisphenol A, as shown in Figure 3e. In addition, benzoic acid was also degraded readily in the Co-Black TNT/PMS system.

The Mechanism of PMS Activation. To confirm the generation of $SO_4^{\bullet -}$ as the main oxidant derived from PMS activation on the TNTs, the kinetics of 4-CP degradation were determined in the presence of excess MeOH, which was used as a $SO_4^{\bullet -}$ scavenger (Figure 4a). The presence of excess MeOH significantly quenched the oxidation of 4-CP in Co-Black TNT, which demonstrates that 4-CP is mainly degraded by $SO_4^{\bullet -}$ generated from PMS activation. Several quinone species including hydroxyhydroquinone (HHQ), hydroquinone (HQ), and benzoquinone (BQ) were found as reaction intermediates during 4-CP oxidation in the Co-Black TNT/PMS system (Figure S9 in the Supporting Information). This result suggests that (i) 4-CP oxidation leads to the generation of chloride and intermediates via attack of $SO_4^{\bullet -}$ generated in Co-Black TNT/PMS system and (ii) $SO_4^{\bullet -}$ radical oxidation also results in the reduction of TOC, as shown in Figure 3c. However, the possible contribution of hydroxyl radical ($^{\bullet}OH$), as quenched by methanol, cannot be ruled out as a contributor to overall oxidation. To confirm this, the quenching effect of MeOH was compared with that of *t*-BuOH in 4-CP degradation by the Co-Black TNT/PMS system. MeOH and *t*-BuOH have a similar bimolecular rate constant for reaction with $^{\bullet}OH$ (9.7×10^8 M^{-1} s^{-1} and 6.0×10^8 M^{-1} s^{-1}, respectively), but the rate constant for MeOH + $SO_4^{\bullet -}$ (3.2×10^6 M^{-1} s^{-1}) is much higher than that for *t*-BuOH + $SO_4^{\bullet -}$ (4.0×10^5 M^{-1} s^{-1}).[13,50] Thus, MeOH and *t*-BuOH scavenge $^{\bullet}OH$ at similar rates, but MeOH is clearly more efficient than *t*-BuOH for $SO_4^{\bullet -}$ scavenging. As shown in Figure S10 in the Supporting Information, the 4-CP degradation was more effectively quenched by MeOH, compared to *t*-BuOH. This result indicates the $^{\bullet}OH$ is a minor contributor to the net degradation of 4-CP degradation in the Co-Black TNT/PMS system. In comparison, the pronounced quenching effects were not observed in the rate of 4-CP degradation on Black TNT. This suggests that 4-CP is mainly oxidized by electron transfer from 4-CP to PMS on the surface of the Black TNT surface.

DOI: 10.1021/acs.est.9b01449
Environ. Sci. Technol. 2019, 53, 6972–6980

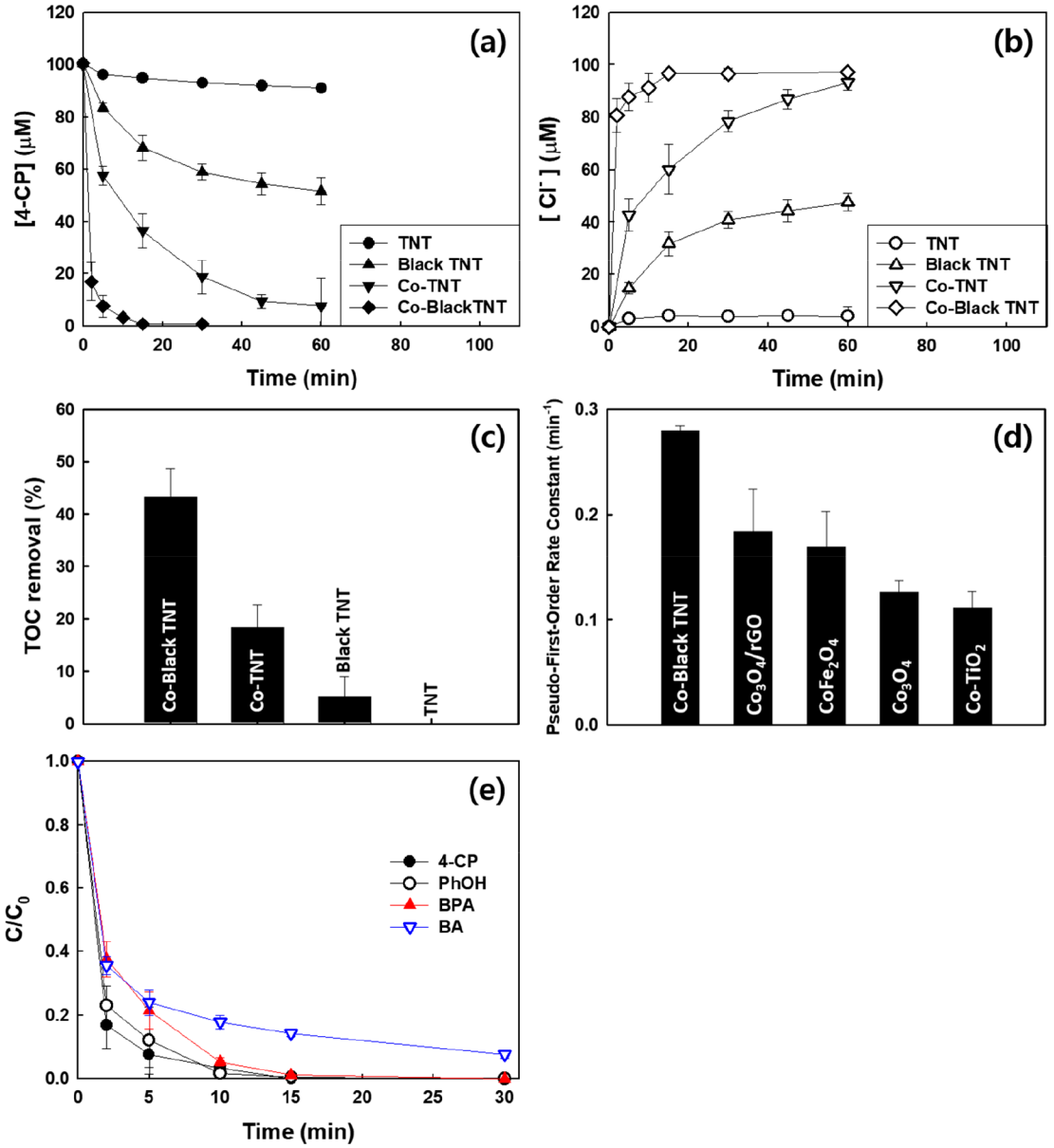

Figure 3. (a) Degradation of 4-CP and (b) production of chloride ions as a result of 4-CP dichlorination and (c) TOC removal after 1 h with TNT, Black TNT, Co-TNT, and Co-Black TNT in the presence of PMS. (c) 4-CP removal by various Co-based materials in the presence of PMS, (d) Oxidative degradation of various organic compounds by PMS activated on Co-Black TNT ([organic pollutants]$_0$ = 100 μM; [PMS]$_0$ = 1 mM; [phosphate buffer]$_0$ = 3 vol %; pH$_i$ = 7.0).

The radical-mediated oxidation processes can also be influenced by NOMs.[20,51,52] The effect of NOM was found to be similar to that of methanol on the degradation of 4-CP by TNTs (see Figure 4b). The 4-CP removal rate was markedly inhibited with different NOMs in the case of the Co-doped TNTs (Co-TNT and Co-Black TNT), while the degradation on Black TNT was not affected by NOM. This result further indicates different reaction pathways for PMS oxidation as catalyzed by Co-doped TNTs, compared to Black TNT. This result clearly shows the role $SO_4^{\bullet-}$ formation pathway on the Co-doped TNTs (i.e., the radical mechanism), compared to the direct electron transfer pathway for 4-CP to PMS (i.e., nonradical mechanism) on the Black TNT. The different PMS activation mechanisms between Co-Black TNT and Black TNT were further demonstrated by PMS decomposition in the presence and absence of 4-CP, as shown in Figure S11 in the Supporting Information. The effect of the electron donor (i.e., 4-CP) is minimized in the radical reaction pathway of Co-Black TNT, while PMS is not effectively decomposed in the absence of an electron donor in the nonradical pathway on Black TNT.[10] The generation of $SO_4^{\bullet-}$ was directly detected using the EPR spin-trapping technique (see Figure 4c). The peaks characteristic of the DMPO–$SO_4^{\bullet-}$ adduct appeared in the EPR spectrum of the Co-doped TNTs. However, the peaks corresponding to 5-*tert*-butoxycarbonyl-5-methyl-2-oxo-pyrroline-1-oxyl (BMPOX), as a product of direct BMPO oxidation,[53] was observed in the case of the bare TNTs and the Black TNTs. The schematic illustration in Figure 4d highlights the role of Co-Black TNT in the activation of PMS, leading to the formation of $SO_4^{\bullet-}$ as a principal oxidant for the degradation of 4-CP (i.e., the radical pathway). In contrast, the Black TNT results in 4-CP oxidation

DOI: 10.1021/acs.est.9b01449
Environ. Sci. Technol. 2019, 53, 6972–6980

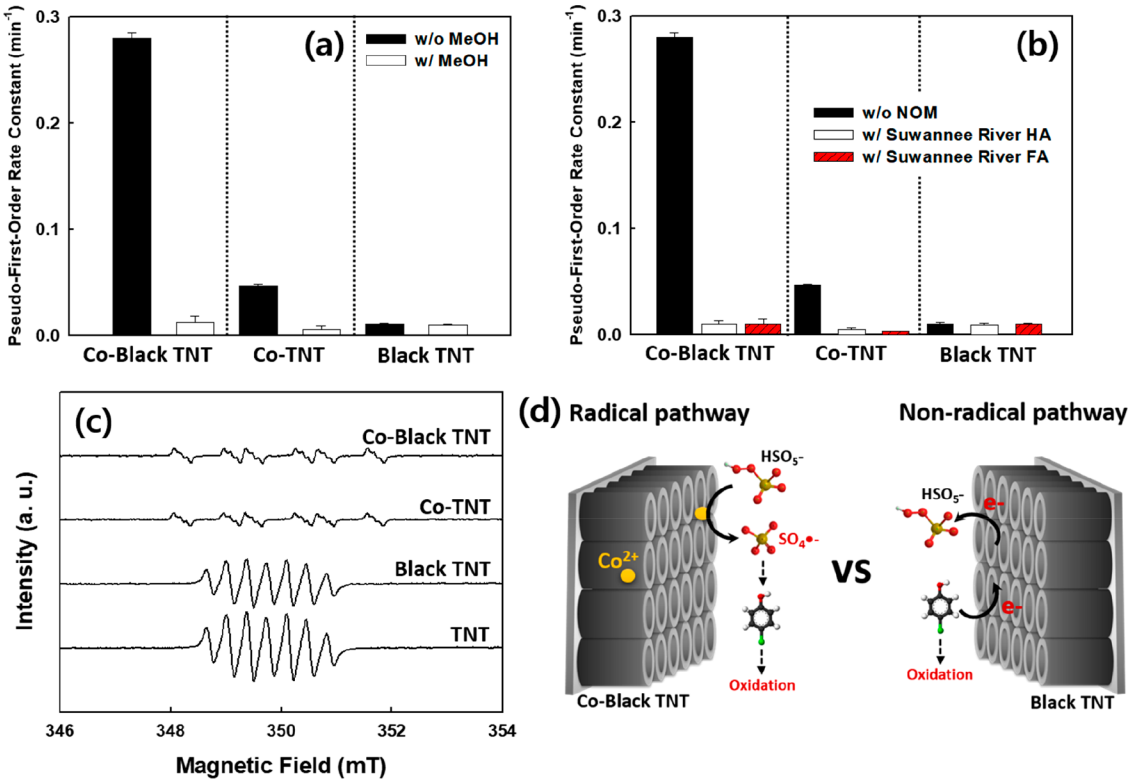

Figure 4. Effect of (a) MeOH and (b) NOM on the rate of 4-CP degradation by PMS activated on TNTs except for bare TNT. (c) EPR spectra obtained in the aqueous BMPO and PMS with TNTs. (d) Schematic illustrations for radical pathway on Co-Black TNT (left) and nonradical pathway on Black TNT (right) for 4-CP degradation. (c) EPR spectra obtained the aqueous BMPO and PMS with TNTs (1 min after PMS activation). $[4\text{-CP}]_0$ = 100 μM (for a); $[\text{MeOH}]_0$ = 100 mM (for a); $[\text{NOM}]_0$ = 10 ppm (for b); $[\text{BMPO}]_0$ = 0.15 mM (for c); $[\text{PMS}]_0$ = 1 mM; [phosphate buffer]$_0$ = 3 vol %; pH_i = 7.0).

via direct electron transfer from 4-CP to PMS (i.e., the nonradical pathway).

Effect of Initial pH on the PMS Activation and Co Leaching. Figure 5 shows the rates of 4-CP degradation in PMS-activated system with Co-doped TNTs, as a function of initial pH. The change in solution pH was not significant over the course of PMS activation. The kinetics of 4-CP degradation maintained in solution pH between 3 and 7. On the other hand, a significant reduction in 4-CP removal was confirmed as the pH increased to 9. An increase in pH to 11 resulted in negligible degradation of 4-CP (pK_a (4-CP = 9.41). This pH-dependent behavior is correlated with the surface charge of Co-doped TNTs. The point of zero charge (PZC) of Co-Black TNT is 5.9 (Figure S12 in the Supporting Information), which is slightly lower than that of TiO_2 (PZC = 6.3).[54] The surface charge of Co-Black TNT is changed from positive to negative with increasing pH, while PMS exists as an anion over a wide pH (i.e., pK_{a1} = 0.4 and pK_{a2} = 9.3).[55,56] The electrostatic repulsion between negatively charged surface of Co-doped TNTs and PMS anion at high pH inhibits the degradation of organic pollutants. The deprotonation of 4-CP (pK_a(4-CP) = 9.41)[57] at high pH results in electrostatic repulsion between the conjugate base of 4-CP and the negatively charged surface of Co-doped TNTs. As a result, the efficiency of 4-CP degradation is significantly reduced at high pH.

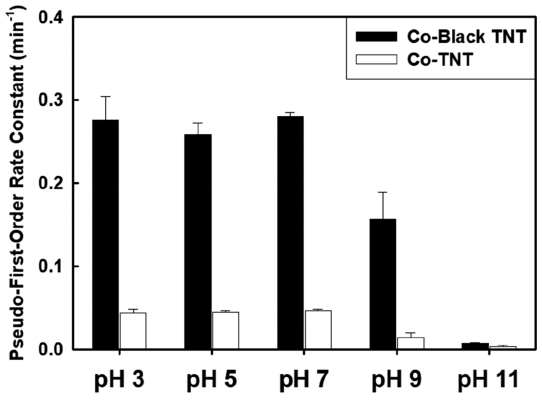

Figure 5. Effect of initial pH on the kinetic rate of 4-CP degradation in PMS activating system with Co-doped TNTs ($[4\text{-CP}]_0$ = 100 μM; $[\text{PMS}]_0$ = 1 mM; pH_i = 3, 5, 7 (buffered using 3 vol % phosphate buffer), 9, and 11).

The effect of initial pH on the leaching of Co^{2+} from the Co-doped TNTs in the presence of PMS. Co^{2+} is readily released from Co_3O_4 in the presence PMS at low pH.[23] The leaching of Co^{2+} from Co-Black TNT and Co-TNT was quantitatively monitored, as a function of pH (Table S1 in the Supporting Information). The loss of Co^{2+} from Co-doped TNTs was found to be negligible (<0.004 mg/L) during PMS activation over a wide pH range. The doping of Co^{2+} into TiO_2 lattice induces strong Co−O−Ti bonds,[58] which essentially prevents the facile leaching of Co^{2+}.

Stability and Recovery of Co-Doped TNTs. In order to confirm the stability of Co-doped TNTs, the degradation of 4-CP was repeated up to 15 cycles for Co-Black TNT and 7 cycles for Co-TNT in the presence of PMS (see Figure 6). The

DOI: 10.1021/acs.est.9b01449
Environ. Sci. Technol. 2019, 53, 6972−6980

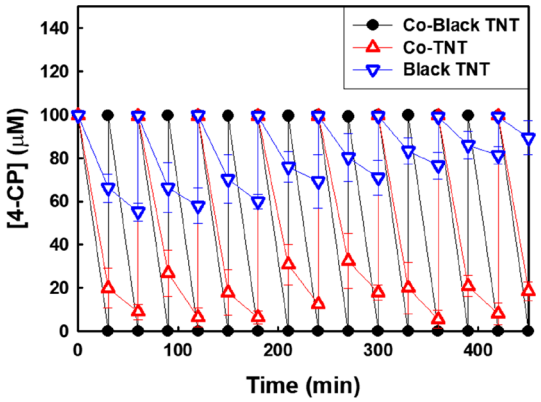

Figure 6. Repeated degradation of 4-CP by PMS activating system with Co-Black TNT, Co-TNT, and Black TNT ($[4\text{-CP}]_0$ = 100 μM; $[PMS]_0$ = 1 mM; $[\text{phosphate buffer}]_0$ = 3 vol %; pH_i = 7.0).

4-CP degradation efficiencies were maintained and the leaching of Co was negligible through multiple uses of both Co-doped TNTs. This result is attributed to the strong bonding of Co−O−Ti in Co-doped TNTs. In particular, Co-Black TNT having surface defect sites (oxygen vacancies and Ti^{3+}) facilitates an efficient redox cycling of the Co ions (Co^{2+}/Co^{3+}) in order to maintain the catalytically active centers (eqs 1 and 2), because of its high electrical and oxygen ion conductivity.[34,35] Therefore, Co-Black TNT/PMS system can be continuously used without the significant deactivation in 4-CP degradation. Co-Black TNT was characterized before and after reaction (10 cycles) (see Figure S13 and accompanying discussion in the Supporting Information for details). Black TNT showed a slight deactivation during repeated PMS activation cycles, which may be due to the accumulation of intermediates generated from 4-CP degradation by the relatively low extent of mineralization (see Figure 3c).

Although many heterogeneous PMS activators have high removal efficiencies and stability, their dispersion in water often hinders the recovery and reuse of catalysts. Co-Black TNTs that are fabricated on and attached to a Ti-metal plate without the use of adhesive substrates or organic binders can be easily recovered from treated water without Co^{2+} leaching and may be reused for multiple catalytic cycles without the need for physical separation and recovery steps (Figure S14 in the Supporting Information). These features may allow for wider use in a variety of water treatment applications using heterogeneous activation of PMS.

Environmental Implications. This study has found that Ti-metal grown Co-Black TNTs provide an efficient, stable, and reusable activation method for harnessing the oxidation potential of PMS for the degradation of organic pollutants. The Co doping of Black TNT leads to the generation of $SO_4^{\bullet -}$ from PMS activation, which could be applied for the oxidative treatment of a broad range of organic chemical contaminants. We have shown that stabilized oxygen vacancies lead to the surficial bonding of PMS to Co-Black TNTs and thus provide the catalytic active sites for the conversion of HSO_5^- to $SO_4^{\bullet -}$. A partial reduction of Ti^{4+} to Ti^{3+} via hydrogenation provides for more-facile electron transfer rates, which further enhances the degradation of organic chemical contaminants. As a result, Co-Black TNTs have a very high efficiency for PMS activation and organic pollutant degradation, compared to other TNT systems. In addition, Co-Black TNTs have practical advantages such as the direct growth of Co-Black TNT on a Ti plate without the need of adhesive substrates or organic binders. The Co-Black TNTs are quite stable with minimal leaching of Co^{2+} into water during the repeated uses. The metal-attached solid-support TNTs can be easily recovered and reused as catalysts in further water treatment applications.

■ ASSOCIATED CONTENT

Supporting Information

The Supporting Information is available free of charge on the ACS Publications website at DOI: 10.1021/acs.est.9b01449.

Experimental details for preparation of four control samples; discussions in Figures S2−S4 and S13; supplementary figures (S1−S14); and Table S1 (PDF)

■ AUTHOR INFORMATION

Corresponding Author

*E-mail: mrh@caltech.edu.

ORCID

Jonghun Lim: 0000-0002-2943-1846

Yang Yang: 0000-0003-3767-8029

Notes

The authors declare no competing financial interest.

■ ACKNOWLEDGMENTS

This research was supported by the Bill and Melinda Gates Foundation (BMGF RTTC Grant Nos. OPP1111246 and OPP1149755).

■ REFERENCES

(1) Anipsitakis, G. P.; Dionysiou, D. D. Degradation of organic contaminants in water with sulfate radicals generated by the conjunction of peroxymonosulfate with cobalt. *Environ. Sci. Technol.* **2003**, *37* (20), 4790−4797.

(2) Rastogi, A.; Al-Abed, S. R.; Dionysiou, D. D. Sulfate radical-based ferrous peroxymonosulfate oxidative system for PCBs degradation in aqueous and sediment systems. *Appl. Catal., B* **2009**, *85* (3−4), 171−179.

(3) Lim, J.; Kwak, D.-y.; Sieland, F.; Kim, C.; Bahnemann, D. W.; Choi, W. Visible light-induced catalytic activation of peroxymonosulfate using heterogeneous surface complexes of amino acids on TiO_2. *Appl. Catal., B* **2018**, *225*, 406−414.

(4) Yun, E.-T.; Yoo, H.-Y.; Bae, H.; Kim, H.-i.; Lee, J. Exploring a role of persulfate in the activation process: Radical precursor versus electron acceptor. *Environ. Sci. Technol.* **2017**, *51*, 10090−10099.

(5) Li, X.; Ao, Z.; Liu, J.; Sun, H.; Rykov, A. I.; Wang, J. Topotactic transformation of metal-organic frameworks to graphene-encapsulated transition-metal nitrides as efficient fenton-like catalysts. *ACS Nano* **2016**, *10*, 11532−11540.

(6) Duan, X.; Sun, H.; Wang, Y.; Kang, J.; Wang, S. N-doping-induced nonradical reaction on single-walled carbon nanotubes for catalytic phenol oxidation. *ACS Catal.* **2015**, *5*, 553−559.

(7) Sun, H.; Liu, S.; Zhou, G.; Ang, H. M.; Tadé, M. O.; Wang, S. Reduced graphene oxide for catalytic oxidation of aqueous organic pollutants. *ACS Appl. Mater. Interfaces* **2012**, *4*, 5466−5471.

(8) Duan, X.; Sun, H.; Kang, J.; Wang, Y.; Indrawirawan, S.; Wang, S. Insights into heterogeneous catalysis of persulfate activation on dimensional-structured nanocarbons. *ACS Catal.* **2015**, *5*, 4629−4636.

(9) Huie, R. E.; Clifton, C. L.; Neta, P. Electron transfer reaction rates and equilibria of the carbonate and sulfate radical anions. *Radiat. Phys. Chem.* **1991**, *38* (5), 477−481.

(10) Ahn, Y.-Y.; Yun, E.-T.; Seo, J.-W.; Lee, C.; Kim, S. H.; Kim, J.-H.; Lee, J. Activation of peroxymonosulfate by surface-loaded noble metal nanoparticles for oxidative degradation of organic compounds. *Environ. Sci. Technol.* **2016**, *50* (18), 10187−10197.

(11) Waldemer, R. H.; Tratnyek, P. G.; Johnson, R. L.; Nurmi, J. T. Oxidation of chlorinated ethenes by heat-activated persulfate: Kinetics and products. *Environ. Sci. Technol.* **2007**, *41* (3), 1010−1015.
(12) Tan, C.; Gao, N.; Deng, Y.; An, N.; Deng, J. Heat-activated persulfate oxidation of diuron in water. *Chem. Eng. J.* **2012**, *203*, 294−300.
(13) Guan, Y.-H.; Ma, J.; Li, X.-C.; Fang, J.-Y.; Chen, L.-W. Influence of pH on the formation of sulfate and hydroxyl radicals in the UV/peroxymonosulfate system. *Environ. Sci. Technol.* **2011**, *45* (21), 9308−9314.
(14) Furman, O. S.; Teel, A. L.; Watts, R. J. Mechanism of base activation of persulfate. *Environ. Sci. Technol.* **2010**, *44* (16), 6423−6428.
(15) Song, H.; Yan, L.; Jiang, J.; Ma, J.; Zhang, Z.; Zhang, J.; Liu, P.; Yang, T. Electrochemical activation of persulfates at BDD anode: Radical or nonradical oxidation? *Water Res.* **2018**, *128*, 393−401.
(16) Matzek, L. W.; Tipton, M. J.; Farmer, A. T.; Steen, A. D.; Carter, K. E. Understanding electrochemically activated persulfate and its application to ciprofloxacin abatement. *Environ. Sci. Technol.* **2018**, *52* (10), 5875−5883.
(17) Anipsitakis, G. P.; Dionysiou, D. D. Radical generation by the interaction of transition metals with common oxidants. *Environ. Sci. Technol.* **2004**, *38* (13), 3705−3712.
(18) Zhang, T.; Chen, Y.; Wang, Y.; Le Roux, J.; Yang, Y.; Croué, J.-P. Efficient peroxydisulfate activation process not relying on sulfate radical generation for water pollutant degradation. *Environ. Sci. Technol.* **2014**, *48* (10), 5868−5875.
(19) Deng, J.; Ya, C.; Ge, Y.; Cheng, Y.; Chen, Y.; Xu, M.; Wang, H. Activation of peroxymonosulfate by metal (Fe, Mn, Cu, and Ni) doping ordered mesoporous Co_3O_4 for the degradation of enrofloxacin. *RSC Adv.* **2018**, *8*, 2338−2349.
(20) Lee, H.; Kim, H.-i.; Weon, S.; Choi, W.; Hwang, Y. S.; Seo, J.; Lee, C.; Kim, J.-H. Activation of persulfates by graphbitized nanodiamonds for removal of organic compounds. *Environ. Sci. Technol.* **2016**, *50*, 10134−10142.
(21) Guan, Y. H.; Ma, J.; Ren, Y.-M.; Liu, Y.-L.; Xiao, J.-Y.; Lin, L.-Q.; Zhang, C. Efficient degradation of atrazine by magnetic porous copper ferrite catalyzed peroxymonosulfate oxidation via the formation of hydroxyl and sulfate radicals. *Water Res.* **2013**, *47*, 5431−5438.
(22) Shukla, P.; Sun, H. Q.; Wang, S. B.; Ang, H. M.; Tade, M. O. Nanosized Co_3O_4/SiO_2 for heterogeneous oxidation of phenolic contaminants in waste water. *Sep. Purif. Technol.* **2011**, *77*, 230−236.
(23) Anipsitakis, G. P.; Stathatos, E.; Dionysiou, D. D. Heterogeneous activation of oxone using Co_3O_4. *J. Phys. Chem. B* **2005**, *109* (27), 13052−13055.
(24) Chen, X.; Chen, J.; Qiao, X.; Wang, D.; Cai, X. Performance of nano- Co_3O_4/peroxymonosulfate system: Kinetics and mechanism study using acid orange 7 as a model compound. *Appl. Catal., B* **2008**, *80* (1−2), 116−121.
(25) Su, S.; Guo, W.; Leng, Y.; Yi, C.; Ma, Z. Heterogeneous activation of oxone by $Co_xFe_{3-x}O_4$ nanocatalysts for degradation of rhodamine B. *J. Hazard. Mater.* **2013**, *244−245*, 736−742.
(26) Yao, Y.; Cai, Y.; Wu, G.; Wei, F.; Li, X.; Chen, H.; Wang, S. Sulfate radicals induced from peroxymonosulfate by cobalt manganese oxides ($Co_xMn_{3-x}O_4$) for fenton-like reaction in water. *J. Hazard. Mater.* **2015**, *296*, 128−137.
(27) Shukla, P. R.; Wang, S.; Sun, H.; Ang, H. M.; Tadé, M. Activated carbon supported cobalt catalysts for advanced oxidation of organic contaminants in aqueous solution. *Appl. Catal., B* **2010**, *100* (3−4), 529−534.
(28) Hu, L.; Yang, X.; Dang, S. An easily recyclable Co/SBA-15 catalyst: Heterogeneous activation of peroxymonosulfate for the degradation of phenol in water. *Appl. Catal., B* **2011**, *102* (1−2), 19−26.
(29) Zeng, T.; Zhang, X.; Wang, S.; Niu, H.; Cai, Y. Spatial confinement of Co_3O_4 catalyst in hollow metal-organic frameworks as a nanoreactor for improved degradation of organic pollutants. *Environ. Sci. Technol.* **2015**, *49* (4), 2350−2357.
(30) Warang, T.; Patel, N.; Fernandes, R.; Bazzanella, N.; Miotello, A. Co_3O_4 nanoparticles assembled coatings synthesized by different techniques for photo-degradation of methylene blue dye. *Appl. Catal., B* **2013**, *132−133*, 204−211.
(31) Yuan, R.; Hu, L.; Yu, P.; Wang, H.; Wang, Z.; Fang, J. Nanostructured Co_3O_4 grown on nickel foam: An efficient and readily recyclable 3D catalyst for heterogeneous peroxymonosulfate activation. *Chemosphere* **2018**, *198*, 204−215.
(32) Weon, S.; Choi, W. TiO_2 nanotubes with open channels as deactivation-resistant photocatalyst for the degradation of volatile organic compounds. *Environ. Sci. Technol.* **2016**, *50*, 2556−2563.
(33) Weon, S.; Choi, J.; Park, T.; Choi, W. Freestanding doubly open-ended TiO2 nanotubes for efficient photocatalytic degradation of volatile organic compounds. *Appl. Catal., B* **2017**, *205*, 386−392.
(34) Yang, Y.; Hoffmann, M. R. Synthesis and stabilization of Blue-Black TiO_2 nanotube arrays for electrochemical oxidant generation and wastewater treatment. *Environ. Sci. Technol.* **2016**, *50*, 11888−11894.
(35) Koo, M. S.; Cho, K.; Yoon, J.; Choi, W. Photoelectrochemical degradation of organic compounds coupled with molecular hydrogen generation using electrochromic TiO_2 nanotube arrays. *Environ. Sci. Technol.* **2017**, *51*, 6590−6598.
(36) Kim, C.; Kim, S.; Lee, J.; Kim, J.; Yoon, J. Capacitive and oxidant generating properties of black-colored TiO_2 nanotube array fabricated by electrochemical self-doping. *ACS Appl. Mater. Interfaces* **2015**, *7*, 7486−7491.
(37) Chen, X.; Liu, L.; Huang, F. Black titanium dioxide (TiO_2) nanomaterials. *Chem. Soc. Rev.* **2015**, *44*, 1861−1885.
(38) Roy, P.; Berger, S.; Schmuki, P. TiO_2 nanotubes: Synthesis and applications. *Angew. Chem., Int. Ed.* **2011**, *50*, 2904−2939.
(39) Paulose, M.; Shankar, K.; Yoriya, S.; Prakasam, H. E.; Varghese, O. K.; Mor, G. K.; Latempa, T. A.; Fitzgerald, A.; Grimes, C. A. Anodic Growth of Highly Ordered TiO_2 Nanotube Arrays to 134 μm in Length. *J. Phys. Chem. B* **2006**, *110*, 16179−16184.
(40) Liang, C. J.; Huang, C. F.; Mohanty, N.; Kurakalva, R. M. A rapid spectrophotometric determination of persulfate anion in ISCO. *Chemosphere* **2008**, *73* (9), 1540−1543.
(41) Zhang, C.; Zhang, L.; Xu, G.; Ma, X.; Xu, J.; Zhang, L.; Qi, C.; Xie, Y.; Sun, Z.; Jia, D. Hollow and core-shell nanostructure Co_3O_4 derived from a metal formate framework toward high catalytic activity of CO oxidation. *ACS Appl. Nano Mater.* **2018**, *1* (2), 800−806.
(42) Yang, Y.; Kao, L. C.; Liu, Y.; Sun, K.; Yu, H.; Guo, J.; Liou, S. Y. H.; Hoffmann, M. R. Cobalt-doped black TiO_2 nanotube array as a stable anode for oxygen evolution and electrochemical wastewater treatment. *ACS Catal.* **2018**, *8*, 4278−4287.
(43) Wang, Y.; Ren, J.; Wang, Y.; Zhang, F.; Liu, X.; Guo, Y.; Lu, G. Nanocasted synthesis of mesoporous $LaCoO_3$ perovskite with extremely high surface area and excellent activity in methane combustion. *J. Phys. Chem. C* **2008**, *112* (39), 15293−15298.
(44) Zhou, W.; Zhao, M.; Liang, F.; Smith, S. C.; Zhu, Z. High activity and durability of novel perovskite electrocatalysts for water oxidation. *Mater. Horiz.* **2015**, *2*, 495−501.
(45) Erdem, B.; Hunsicker, R. A.; Simmons, G. W.; Sudol, E. D.; Dimonie, V. L.; El-Aasser, M. S. XPS and FTIR surface characterization of TiO_2 particles used in polymer encapsulation. *Langmuir* **2001**, *17*, 2664−2669.
(46) Lim, J.; Monllor-Satoca, D.; Jang, J. S.; Lee, S.; Choi, W. Visible light photocatalysis of fullerol-complexed TiO_2 enhanced by Nb doping. *Appl. Catal., B* **2014**, *152−153*, 233−240.
(47) Pan, X.; Yang, M.-Q.; Fu, X.; Zhang, N.; Xu, Y.-J. Defective TiO_2 with oxygen vacancies: Synthesis, properties and photocatalytic applications. *Nanoscale* **2013**, *5*, 3601−3614.
(48) Su, C.; Duan, X.; Miao, J.; Zhong, Y.; Zhou, W.; Wang, S.; Shao, Z. Mixed conducting perovskite as superior catalysts for fast aqueous-phase advanced oxidation: A mechanistic study. *ACS Catal.* **2017**, *7*, 388−397.
(49) Ji, Y.; Kilner, J. A.; Carolan, M. F. Electrical conductivity and oxygen transfer in gadolinia-doped ceria (CGO)-$Co_3O_{4-\delta}$ composites. *J. Eur. Ceram. Soc.* **2004**, *24*, 3613−3616.

DOI: 10.1021/acs.est.9b01449
Environ. Sci. Technol. 2019, 53, 6972−6980

(50) Neta, P.; Huie, R. E.; Ross, A. B. Rate constants for reactions of inorganic radicals in aqueous solution. *J. Phys. Chem. Ref. Data* **1988**, *17* (3), 1027−1284.
(51) Liu, F.-f.; Fan, J.-l.; Wang, S-g.; Ma, G.-h. Adsorption of natural organic matter analogues by multi-walled carbon nanotubes: Comparison with powdered activated carbon. *Chem. Eng. J.* **2013**, *219*, 450−458.
(52) Lindsey, M. E.; Tarr, M. A. Inhibition of hydroxyl radical reaction with aromatics by dissolved natural organic matter. *Environ. Sci. Technol.* **2000**, *34* (3), 444−449.
(53) Ahn, Y.-Y.; Bae, H.; Kim, H.-i.; Kim, S.-H.; Kim, J.-H.; Lee, S.-G.; Lee, J. Surface-loaded metal nanoparticles for peroxymonosulfate activation: Efficiency and mechanism reconnaissance. *Appl. Catal., B* **2019**, *241*, 561−569.
(54) Kim, J.; Lee, C. W.; Choi, W. Platinized WO_3 as an environmental photocatalyst that generates OH radicals under visible light. *Environ. Sci. Technol.* **2010**, *44* (17), 6849−6854.
(55) Elias, H.; Götz, U.; Wannowius, K. J. Kinetics and mechanism of the oxidation of sulfur (IV) by peroxomonosulfuric acid anion. *Atmos. Environ.* **1994**, *28*, 439−448.
(56) Evans, D. F.; Upton, M. W. Studies on singlet oxygen in aqueous solution. Part 3. The decomposition of peroxy-acids. *J. Chem. Soc., Dalton Trans.* **1985**, *0*, 1151−1153.
(57) Serjeant, E. P.; Dempsey, B. *Ionisation Constants of Organic Acids in Aqueous Solutions*; IUPAC Chemical Data Series, No. *23*; Pergamon: Oxford, U.K., 1979.
(58) Zhu, Y.; Chen, S.; Quan, X.; Zhang, Y. Cobalt implanted TiO_2 nanocatalyst for heterogeneous activation of peroxymonosulfate. *RSC Adv.* **2013**, *3*, 520−525.

DOI: 10.1021/acs.est.9b01449
Environ. Sci. Technol. 2019, 53, 6972−6980